PAPER

Check for updates

Enantioselective effect of cysteine functionalized mesoporous silica nanoparticles in U87 MG and GM08680 human cells and *Staphylococcus aureus* bacteria†

Marina Martínez-Carmona, [ID] *[a] Carmela Cela, [ID] [a] Vera A. Kuznetsova,[a] Joan A. Geoghegan [ID] [bc] and Yurii K. Gun'ko [ID] [a]

Chirality is a fundamental phenomenon in biological systems, since most of the biomolecules and biological components and species are chiral and therefore recognize and respond differently depending on the enantiomer present. With increasing research into the use of nanomaterials for biomedical purposes, it is essential to understand the role that chirality of nanoparticles plays at the cellular level. Here, the chiral cysteine functionalization of mesoporous silica nanoparticles has been shown to broadly affect its interaction with U87 MG human glioblastoma cell, healthy human fibroblast (GM08680) and methicillin-resistant *S. aureus* bacteria. We believe that this research is important to further advancement of nano-biotechnology.

Introduction

The use of nanoparticles for biomedical purposes has been at the pipeline of research for several decades.[1–3] Initially research was mostly focused on the new advantages and properties that arise in existing materials when reducing the size to nanometric scale.[4] But over time a lot of effort has been invested in functionalizing them with different molecules, polymers, proteins, antibodies, aptamers, *etc.* seeking to improve their selectivity[5–7] or action as a consequence of a stimulus/response.[8–11] It was possible to produce complex systems capable of fulfilling very specific functions and in many cases of great scientific value. However, for accomplishing great feats, we sometimes forget to pay enough attention to small but vital details. This is the case of chirality in nanoparticles, despite the time that nanomedicine has been studied, little attention has been paid into knowing how this phenomenon affects interaction with biological systems.

Presence of chirality in nature is undeniable, many molecules of living organism possess a particular enantiomeric configuration, for example human proteins are made of L-amino acids, while D-configuration predominates in carbohydrates.[12] The importance of chirality in biological systems resides in molecular recognition processes, where enzymes and cell receptor molecules can distinguish two enantiomeric substrates. Therefore, enantiomers are likely to experience selective biochemical interactions such as absorption, distribution, metabolism and elimination.[13] Molecular recognition is a key feature when developing chiral drugs, since enantiomers can have very different effects. A very well-known case is thalidomide, in which the *S*-enantiomer is teratogenic while the *R*-form has sedative effects.[14]

Since chirality is such a fundamental property of a living organism and the chiral recognition is crucial for understanding of effects of chiral drugs, the study of chirality in nanomaterials for biomedical applications is a very important research topic. Recently, this issue has been addressed by a few of scientific publications which reveals the increasing interest that the nanomedicine field is putting onto it. In this respect, there are some previous reports that show clear evidences of the effect of chirality in nanomaterials on molecular recognition,[15] cell migration, cell adhesion or DNA replication inhibition.[16–22]

For instance, Li *et al.* reported that regardless of size, when functionalized QDs with chiral glutathione (GSH), the autophagy and cytotoxicity in HepG2 cells was greater for L-GSH-QDs than for D-GSH-QDs.[23] In a different study performed by Deng *et al.*, it was shown that, after binding to gold nanoparticles, the D form of

[a] *School of Chemistry, CRANN and AMBER Research Centres, Trinity College Dublin, College Green, Dublin 2, Ireland. E-mail: marina.m.c1@um.es*

[b] *Department of Microbiology, Moyne Institute of Preventive Medicine, School of Genetics and Microbiology, Trinity College Dublin, Dublin, Ireland*

[c] *Institute of Microbiology and Infection, College of Medical and Dental Sciences, University of Birmingham, B15 2TT Birmingham, UK*

† Electronic supplementary information (ESI) available: COOH-MSN SEM image, FTIR spectra of COOH-MSN (before and after CTAB extraction), D-Phen MSN and L-Phen MSN, DLS of the NPs, TEM-EDX of the functionalized NPs, CD spectra of D/L Cys, D/L-Cys MSN, D/L Phen and D/L-Phen MSN, Newman projections of right and left binding conformations Phen molecules on the MSN surface, internalization and toxicity of plain MSN in U87 MG cells, flow cytometry data of D/L-Cys MSN and D/L-Phen MSN in U87 MG cells, flow cytometry data of D/L-Cys MSN and D/L-Phen MSN in healthy human fibroblast (GM08680) and flow cytometry data of D/L-Cys MSN and D/L-Phen MSN in *S. aureus* bacteria. See DOI: 10.1039/d0tb02532a

3544 | *J. Mater. Chem. B*, 2021, **9**, 3544–3553

This journal is © The Royal Society of Chemistry 2021

poly(acryloyl-L(D)-valine) enhanced the uptake by A549 and HepG2 cells.[24] Similar studies have also been carried out on the influence exerted by the chirality of nanoparticles on bacteria.[25,26] Most of the papers are devoted to chiral metal NPs,[27,28] but there are also publications on polymeric nanoparticles,[29,30] carbon nanoparticles[31,32] or selenium ones[26] among others. Mesoporous silica nanoparticles (MSN) have proven to be a great resource for the treatment of several diseases such as bacterial infection,[33,34] cancer,[35] Alzheimer,[36] *etc.* Nevertheless, there are still many open questions to address the influence of chirality of MSN for interaction with biological systems. For example, Rosen *et al.* characterized the physicochemical properties of zwitterionic L-cysteine (Cys) functionalized silica nanoparticles.[37] They found that cysteine coating provided the nanoparticles a higher stability in biological media such as human serum, but no studies were performed on the effect that chirality plays in stability and neither in cell-interaction or cytotoxicity. Another study by Guo *et al.*, showed that chirality influences drug release.[38] MSN were functionalized with either D or L-tartaric acid. D-MSN showed a higher and sustained drug release over time, and hence a stronger pharmacodynamic performance *in vivo.* Also related to the selective drug release is the study carried out by Fan *et al.*,[39] who synthesized on–off chiral MSN able to deliver achiral drug indometacin in chiral environment.

As a very promising antecedent of our work, Li *et al.* reported how the functionalization of L-Cys MSN allows to selectively target the Golgi apparatus in Hep-2 cells.[40] Although this work presented chiral characterization by circular dichroism of D and L-Cys MSN, it did not compare the different biological behaviour of the enantiomers, hence they did not explore the influence of chirality in their biological system. In this respect, to go beyond the current state of the art in cell chiral-MSN interactions,[41–43] in this work we not only use chiral amino acid functionalized MSN in two different biological systems, but we also compare the different behaviour they present depending on their chirality. Cysteine functionalisation was previously reported by Rosen *et al.* to be stable in biological media,[37] which is fundamental for nanomedicine approaches. Thereupon, here we report the preparation and characterization of the chiral cysteine (Cys) functionalization of mesoporous silica nanoparticles and investigate their cell-interaction with U87 MG human glioblastoma cells, healthy human fibroblast (GM08680) and methicillin-resistant *S. aureus* bacteria. Phenylalanine (Phe) MSN were used as a control, as we found that this functionalization did not confer chiral properties to the nanoparticles. The selectivity and efficacy of D-Cys MSN in U87 cells, together with the ability to load antitumor drugs inside the pores, make this nanodevice a powerful tool to combat neuroblastoma.

Experimental

Reagents

All chemical reagents were of analytical grade and used as purchased without further purification. Tetraethylorthosilicate (TEOS, 98%), *n*-cetyltrimethylammonium bromide (CTAB, ≥99%), sodium hydroxide (NaOH, ≥98%), ammonium nitrate (NH$_4$NO$_3$, ≥98%), sodium carbonate (Na$_2$CO$_3$, ≥99.5%), hydrochloric acid (HCl, 37%), fluorescein 5(6)-isothiocyanate (FITC, ≥98%), rhodamine B isothiocyanate (RITC, ≥98%), (3-aminopropyl)triethoxysilane (APTES, ≥98%), *N*-(3-dimethylaminopropyl)-*N*′-ethylcarbodiimide hydrochloride (EDAC, ≥98%), 3-(triethoxysiyl)propylsuccinic anhydride (SATES, 95%) were purchased from Sigma-Aldrich. Ethanol and distilled water (Millipore) were used as solvents.

Characterization techniques

Fourier transform infrared spectroscopy (FTIR) was carried out in a Nicolet (Thermo Fisher Scientific, Waltham, MA, USA) Nexus spectrometer equipped with a Goldengate attenuated total reflectance (ATR) accessory (Thermo Electron Scientific Instruments LLC, Madison, WI, USA). Morphology was studied by High Resolution Transmission Electron Microscopy (HRTEM) with a JEOL JEM 3000F instrument operating at 300 kV, equipped with a CCD camera (JEOL Ltd, Tokyo, Japan). Sample preparation was performed by dispersing in EtOH and subsequent deposition onto carbon-coated copper grids. SEM-EDX analysis was performed on a JEOL 6100 (Japan) instrument operating at 20 kV. Sample preparation was performed by powder deposition onto a copper stud, dried and coated with a film of gold previous observation. Thermogravimetric (TG measurements) were performed in a PerkinElmer Pyris Diamond TG/DTA (California, USA), (heating from 25 °C to 100 °C at 10 °C min^{-1}, hold for 5 min at 100 °C to remove all remained water and heat from 100 °C to 900 °C). To determine the evolution of the size and surface charge of nanoparticles by dynamic light scattering (DLS) and zeta (ζ)-potential measurements, respectively, a Zetasizer Nano ZS (Malvern Instruments, United Kingdom) equipped with a 633 nm "red" laser was used. DLS and ζ-potential measurements were recorded in aqueous colloidal suspensions. For this purpose, 1 mg of nanoparticles was added to 10 mL of solvent followed by 5 min of sonication to obtain a homogeneous suspension. Measurements were recorded by placing 1 mL of suspension (0.1 mg mL^{-1}) in DTS1070 disposable folded capillary cells (Malvern Instruments).

Synthesis of fluorescent COOH-MSN

COOH-MSN have been synthesized by a 'co-condensation' synthesis method. 1 g of CTAB, 480 mL of H$_2$O and 3.5 mL of NaOH (2 M) were added to a 1000 mL round-bottom flask. The mixture was heated to 80 °C and magnetically stirred at 600 rpm. Meanwhile, 1 mg FITC and 2.2 μL APTES were dissolved in 100 μL ethanol and left reacting for 2 h. After that, the FITC reaction mixture was mixed with 4 mL of TEOS and 1.26 mL of SATES and added dropwise at 0.33 mL min^{-1} rate to the CTAB solution. The yellowish suspension obtained was stirred for 2 h at 80 °C. The nanoparticles were collected by centrifugation, washed twice with water and resuspended in 500 mL of a NH$_4$NO$_3$ solution (10 mg mL^{-1}) in ethanol (95%) at 65 °C overnight under magnetic stirring to remove the surfactant. The calcination method was not chosen to avoid partial condensation between nanoparticles.[44] The MSN were collected by centrifugation, washed twice with water and twice with ethanol

This journal is © The Royal Society of Chemistry 2021

J. Mater. Chem. B, 2021, **9**, 3544–3553 | **3545**

and finally stored in an ethanol suspension to avoid aggregation or the nanoparticles dissolution.[45]

Non fluorescent COOH-MSN was synthesized for antimicrobial experiments. The synthesis process was analogous to that described above but in the absence of the silylated FITC.

Functionalization with L-/D-cysteine and L/D phenylalanine

Following the procedure described by Shieh et al.,[46] 100 mg of COOH-MSN were suspended in 12 mL of MilliQ water and subjected to several sonication cycles of 5 min until a good suspension was achieved. Then, 28 755 mg of EDAC (0.15 mmol) and 35 μL of triethylamine (0.25 mmol) were added and stirred for 30 min. After that, 8 mL of a solution of 0.05 M of the amino acid (L-/D-Cys or Phen) was gently added to the suspension and the mixture was reacted overnight. The product was filtered washed twice with water and twice with ethanol and storage in an ethanol suspension. Before adding to the cells, nanoparticles were washed twice with water and once with the proper culture media.

Cell culture

U87 MG human glioblastoma and human skin fibroblasts from healthy donors (GM08680) cell lines were cultured in Minimum Essential Medium Eagle (MEM) (Sigma-Aldrich) supplemented with 10% FBS under humidified atmosphere of 5% CO_2 at 37 °C. Additionally, U87 MG was supplemented with 1% L-glutamine and GM08680 was supplemented with antibiotics (100 mg L^{-1} streptomycin and 200.000 U L^{-1} penicillin). For all the experiments, the cells were seeded on 24 well plates in an initial density of 25 000 cells per well and left to attach for 24 h.

Internalization assays of nanoparticles in U87 MG

After 24 h, cells were incubated with medium containing different concentrations of the chiral nanoparticle suspensions (100, 50, 25 and 5 μg mL^{-1}). After 2 h, cells were washed twice with PBS and incubated at 37 °C with trypsin–EDTA solution (Sigma-Aldrich) for cell detachment. The reaction was stopped with culture medium after 5 min and cells were centrifuged at 1000 rpm for 10 min and resuspended in fresh PBS containing 1 μL mL^{-1} of SYTO red (SYTO 60 red fluorescent nucleic acid stain dye). After 10 min flow cytometry measurements were performed at an excitation wavelength of 488 nm, green fluorescence was measured at 530 nm (FL1). The trigger was set for the green fluorescence channel (FL1). The conditions for the data acquisition and analysis were established using negative and positive controls with the CellQuest Program of Becton–Dickinson and these conditions were maintained during all the experiments. Each experiment was carried out three times and single representative experiments were displayed. Then, the surface fluorescence of the cells was quenched with trypan blue (0.4%) to confirm the presence of an intracellular, and therefore internalized, fluorescent signal. After that, the flow cytometry experiments were repeated.

Internalization assays of nanoparticles in GM08680

After 24 h, cells were incubated with medium containing different concentrations of the chiral nanoparticle suspensions (100, 50, 25 and 5 μg mL^{-1}). After 2 h, cells were washed twice with PBS and incubated at room temperature with trypsin–EDTA solution for 5 min for cell detachment. The reaction was stopped with culture medium and cells were centrifuged at 1500 rpm for 5 min. Cells were washed with 100 μL of PBS 1× and then resuspended in 200 μL staining PBS. Following flow cytometry measurements were performed using the same settings as previously described.

Cell viability of nanoparticles against U87 MG

Cell viability was analyzed using the Cell Counting Kit-8 (CCK-8) (Dojindo, Europe). Cells were cultured as described above without (control) or with the tested materials (L-/D-Cys or Phen MSN) at different concentrations (100, 50, 25 and 5 μg mL^{-1}). After the incubation period (24 or 48 h), cell viability was evaluated. The reagent was directly mixed with fresh media and put in contact with the cells for 1 h at 37 °C. After that, the absorbance at 450 nm was read. The viability was plotted as percentage (%) of absorbance normalized for the controls.

Cell viability of nanoparticles against GM08680 MG

Cell viability was analyzed by flow cytometry using 7-amino-actinomicina D (7-AAD) (BD-Biosciences) which only penetrates death cells. Cells were cultured as described above, without (control) or with the tested materials (L-/D-Cys or Phen MSN) at different concentrations (100, 50, 25 and 5 μg mL^{-1}). After the incubation period (24 or 48 h), cell viability was evaluated. Cells were detached, washed as resuspended in staining PBS as previously described. Viability reagent 7-AAD was directly added to the cells when resuspended in staining PBS and incubated during 15 min at room temperature. After that, flow cytometer measurements were performed at an excitation wavelength of 546 nm and emission fluorescence was measured at 647 nm (FL3). The viability was plotted as percentage (%) of negative 7-AAD fluorescence normalized for the controls.

Internalization assays into S. aureus planktonic bacteria

Culture conditions. S. aureus (strain BH1CC MRSA)[47] was grown in tryptic soy broth (TSB) at 37 °C for approximately 16–18 h. The bacterial suspension was centrifuged at maximum power for 5 min and 1 mL of fresh PBS was added to carefully resuspend the cells. The suspension was diluted to adjust the optical density at 600 nm to 0.35. One millilitre was transferred to a clean tube, the washing protocol was repeated twice and finally bacteria were resuspended in 1 mL of PBS.

Treatment conditions

D/L-Cys, D/L-Phen functionalized fluorescent MSN were added to 50 μL of bacteria suspension to reach final concentrations of 5, 25, 50 and 100 μg mL^{-1}. The samples were incubated for 90 min with shaking (200 rpm) at 37 °C and then centrifuged at maximum power for 5 min. The supernatant was removed,

3546 | J. Mater. Chem. B, 2021, **9**, 3544–3553

This journal is © The Royal Society of Chemistry 2021

and the pellet was washed with 50 µL of PBS without resuspending it. Next, internalization was measured by flow cytometry. To do so, 50 µL of the red SYTO red dye were added and incubated for 10 min at room temperature (RT). The samples were washed with 500 µL of PBS. Finally, 600 µL of PBS-formaldehyde 2% were added to fix the cells. After 10 min, flow cytometer measurements were performed following the same protocol as in the internalization in glioblastoma cells experiment.

Antimicrobial effects against *S. aureus* planktonic bacteria

Culturing and treating conditions were the same as explained previously for internalization experiments in planktonic bacteria. Non-fluorescent MSN were used instead to avoid fluorescence interference with the viability kit that we used (LIVE/DEAD™ BacLight™ Bacterial Viability Kit). D/L-Cys, D/L-Phen functionalised non-fluorescent MSN in final concentrations of 5, 25, 50 and 100 µg mL^{-1} were used. After incubation and washing, cell viability was measured using the viability kit mentioned above. Flow cytometer measurements were performed without fixing the cells at an excitation wavelength of 480 nm and green fluorescence was measured at 500 nm (FL1).

Internalization assays into *S. aureus* bacteria biofilm

S. aureus MRSA (BH1CC) was transformed with plasmid pCM29[35] expressing Green Fluorescent Protein (GFP) using electroporation. BH1CC (pCM29) was grown in TSB for 16–18 h and then subcultured 1 : 200 into brain heart infusion (BHI) broth supplemented with glucose (1% wt/v) in a six well flat-bottomed tissue culture plate and incubated statically at 37 °C for 6 h (early biofilm) or 18 h (mature biofilm).

After that, D/L-Cys, D/L-Phen functionalized MSN were added in a final concentration of 100 µg mL^{-1} in PBS. These MSN were previously loaded with Rhodamine B red fluorophore in order to be able to trace them in the GFP expressing bacterial biofilm. Since our aim was to study the effect of chirality in internalization, we used nonfunctionalized MSN containing Rhodamine B by co-condensation synthesis, as a control. Three different incubation times were set: 90 min, 6 h and 18 h. The loading protocol consisted in preparing 10 mg of each type of nanoparticles and place them into 1 mL of Rhodamine B solution (1 mg mL^{-1}) with magnetical stirring at RT overnight. Rhodamine B excess was removed by centrifuging and washing the samples with water until the supernatant was clear.

Results and discussion

Preparation and characterization of the nanosystems

The chiral nanoparticles were synthesized in two steps. Firstly, COOH-MSN were synthetized by co-condensation of SATES and TEOS using the modified Stöber method.[48] Structural characterization by SEM shows an average size of the particles around 120 nm. It is also noticed that the presence of 20% in SATES slightly modifies the typical spherical shape of the MCM-41 silica nanoparticles (Fig. S1, ESI†). After that, the nanoparticles

were externally functionalized by the reaction between the amine groups present in L-/D-cysteine and L-/D-phenylalanine and the carboxylic acid of the nanoparticles. All types of nanoparticles were characterized by various instrumental techniques and compared with initial COOH-MSN. FTIR spectroscopy (Fig. S2, ESI†) of COOH-MSN showed the absence of the CTAB peaks (2.922 and 2.855 cm^{-1}) confirming the removal of the template.[49] Additionally, in Fig. 1 the characteristic stretching vibration of carboxylic acid groups (1750 cm^{-1}), which practically disappears after cysteine or phenylalanine (Fig. S3, ESI†) functionalization, giving way to the amide bonds (1580 and 1540 cm^{-1}) and NH out-of plane (700 to 600 cm^{-1}) bands, confirming the satisfactorily functionalization for all type of nanoparticles.[34]

The decrease in ζ-potential measurements (from −11.0 for COOH-MSN to −19.4, −20,3, −16.1 and −14.2 mV for L/D-Cys-MSN and L/D-Phen-MSN respectively) after the functionalization is in agreement with these results. For each bond that is formed, the surface of the particles lose a COOH group, which is finally overcompensated by the COOH and SH groups provided by the incorporated cysteine. Phe, not having SH, produces a smaller change in potential. The mean hydrodynamic sizes determined by DLS were found to be 141 nm, around 160 nm and around 191 nm for COOH-MSN, D/L-Cys MSN and D/L-Phen MSN (Fig. S4, ESI†). As expected, the hydrodynamic sizes, that include the solvation layer, are slightly higher than the one estimated from TEM images.[50,51] The percentage of functionalization was calculated by thermogravimetric analysis and turned out to be approximately 8% for both D/L-Cys samples and 5% for the Phen ones. Additionally, TEM–EDX analysis of the amino acids functionalized samples were also performed (Fig. S5, ESI†). S was detected in the L/D-Cys-MSN samples confirming the presence of Cys on the nanoparticles surface. However, the presence of lighter elements such as C, N, was not detectable, suggesting that the values were below the detection limit of the equipment. As expected, these same elements were neither detected in the L/D-Phen-MSN samples with slightly lower functionalization. The chirality of the nanoparticles was studied by circular dichroism spectroscopy.
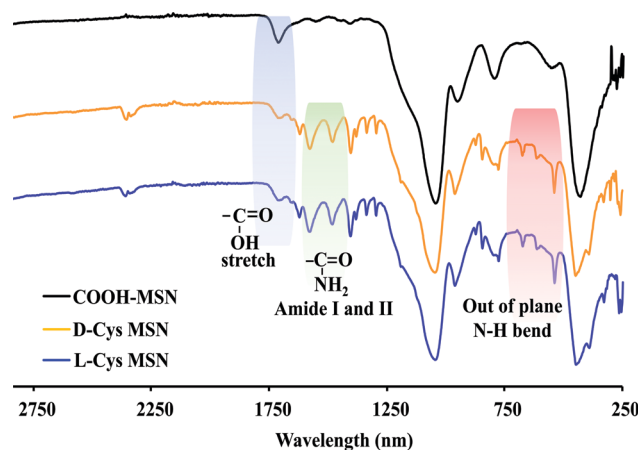

Fig. 1 FTIR spectra of COOH-MSN (black), D-Cys-functionalized MSN (orange) and L-Cys functionalized MSN (blue).
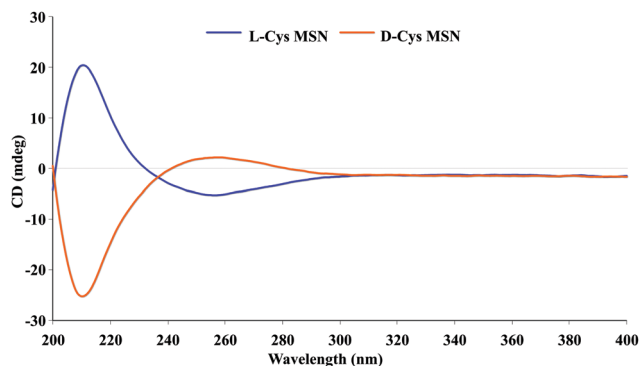
This journal is © The Royal Society of Chemistry 2021

J. Mater. Chem. B, 2021, **9**, 3544–3553 | **3547**

Fig. 2 CD spectra of D-Cys-functionalized MSN (orange) and L-Cys functionalized MSN (blue).

The cysteine functionalized MSN were chiroptically active, which was reflected in the appearance of mirror-imaged CD signals for both samples (Fig. 2) comparable to that of the free molecules (Fig. S6, ESI†). However, the Phen-functionalized nanoparticles showed no chirality (Fig. S7, ESI†). The reason could be that Phen can have two binding conformations on the surface of the MSN, which are stereoisomers of each other. In this case, they have an opposite CD signal and compensate each other. Many examples of stereoisomer binding modes for other amino acids are known in the literature.[15,52–54]

Initially, the MSN surface is functionalized with carboxyl groups, which are further bound to amino groups of Phen. Wherein the carboxyl and phenyl groups of Phen remain free. Free carboxyl groups can bind to amino groups of neighboring Phen molecules by hydrogen bonds. While phenyl groups of neighboring molecules can bind with each other via π–π stacking, forming pairs in which the Phen of one molecule is directed to the right, and the second to the left, towards each other, have binding conformations corresponding to the opposite stereoisomers of Phen (Fig. S8, ESI†).

Effect of chirality in U87 MG

Firstly, to know the effect that the transporter itself exerted on cells, control was performed with non-functionalized nanoparticles. To study internalization U87 MG cells were incubated with 50 μg mL^{-1} of plain fluorescent NPs for 2 hours. After that, the media was changed to remove the non-internalized nanoparticles and cells were observed by confocal microscopy. As can be seen in Fig. S9 (ESI†) these nanoparticles produced negligible internalization, which is consistent with previously published results.[55] Additionally, the cytotoxicity of the NPs against U87 cells was studied. Fig. S10 (ESI†) shows that no significant cytotoxicity was observed for concentrations up to 100 μg mL^{-1} even after 72 h of treatment.

In order to test whether the chirality of the cysteine molecule affects the internalization and/or toxicity of the nanoparticles, two complementary studies were performed. To study the effect on the internalization, U87 MG cells were incubated in the presence of fluorescent L-/D-Cys MSN. Thus, U87 MG cells were exposed to a certain amount (5, 25, 50 and 100 μg mL^{-1}) of
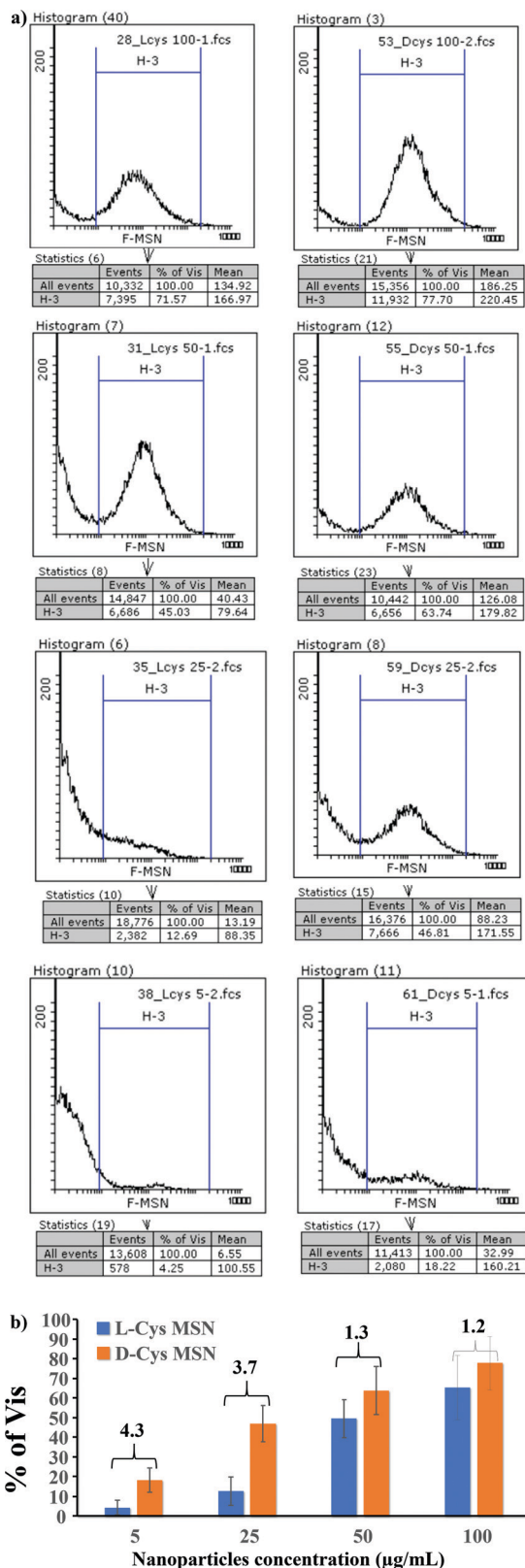

Fig. 3 (a) Histogram of the internalization of fluorescent L-/D-Cys-MSN in U87 MG at different incubation concentrations (5, 25, 50 and 100 μg mL^{-1}) of. (b) Evolution of internalization as a function of concentration.

fluorescent nanoparticles for 2 hours (Fig. S11, ESI†). The percentage of cells which engulf particles was determined by flow cytometry (Fig. 3a). Both types of nanoparticles presented a concentration-dependent fluorescence. However, significant differences were observed depending on the chirality of the molecule. D-Cys MSN show a 4.3-fold increase in cell uptake in comparison with L-Cys MSN for the concentration of 5 μg mL^{-1}. This difference was gradually reduced as the concentration increased, acquiring a value of 1.2 for the concentration of 100 μg mL^{-1} (Fig. 3b). After that, trypan blue was added to the cells, 10 min later the flow cytometry experiments were repeated.[56] As can be seen in Fig. S12 (ESI†), the results coincide with those obtained before addition of trypan blue, indicating that fluorescence came from inside the cells and not from particles adhered to the surface.

This data agrees with the phenomenon observed by Guo *et al.*, in which D-enantiomer coated NP internalization was more prevalent than internalization of L-enantiomer coated NP.[38] In this work they suggested that this is likely to occur because L-phospholipid-based cell membrane has a preferable interaction with the D-enantiomer coating.

The second experiment was performed to evaluate the viability of the cells in the presence of different nanoparticles concentrations (5, 25, 50 and 100 μg mL^{-1}). The results indicate that cell death induced by D-Cys MSN is higher than the one produced by L-Cys MSN (Fig. 4). This difference is more evident for the lower concentrations (5 μg mL^{-1}) and is reduced when increasing the concentration and even equals for higher concentrations.

These results are consistent with the internalization patterns observed in both types of particles, suggesting that the accumulation inside the cell is responsible for cell death.

Furthermore, our results for D-Cys MSN are in line with previously published results where D-Cys QDs caused greater toxicity against A549 cells.[57] The mechanism of cell death induced by silica nanoparticles *in vitro* is still not completely clear. Some authors attribute it to reactive oxygen species (ROS) production.[58,59] Others agree that cytotoxicity of silica into human cells highly depends on cell metabolic activity.[60] In this respect, a study by Kretowski *et al.* performed in glioblastoma cell lines similar to U87 MG showed apoptosis and autophagy induced by silica nanoparticles. They proposed a mitochondrial-dependent pathway of apoptosis as the cell death mechanism mediated by silica nanoparticles.[61]

The same experiments were performed with the Phen functionalized nanoparticles that did not show chirality. Fig. S13 and S14 (ESI†) show that the internalization in U87 cells was superior for Phen-NPs than for Cys-NPs, however, there were no differences between L and D forms. Regarding the toxicity, no significant differences were observed between L/D Phen functionalized NPs (Fig. S15, ESI†), with the exception of a small increase detected 24 h after adding L-Phen in a concentration of 25 μg mL^{-1}. However, taking into account the size of the error bar and that this difference disappears after 48 hours, it can be considered irrelevant. This observation stresses the relevance of chirality in MSN–cell interaction, since chiral
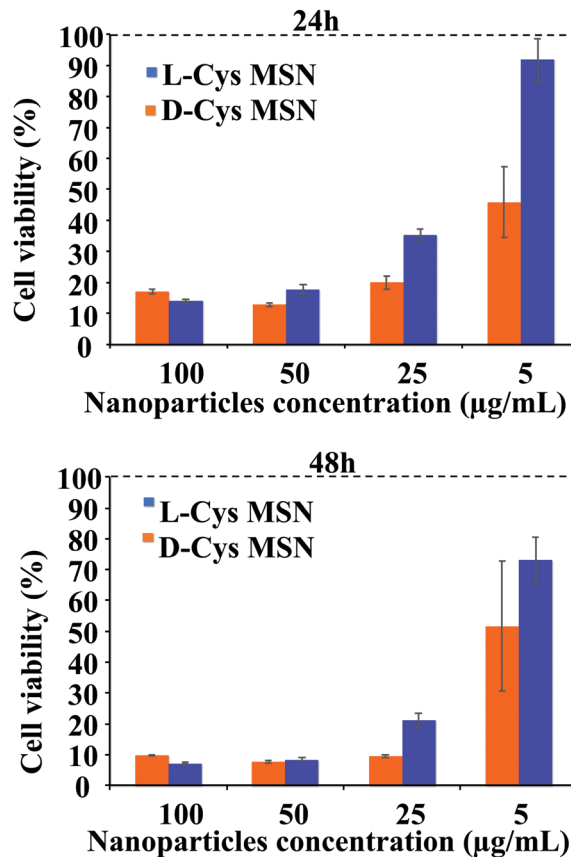

Fig. 4 Cytotoxicity assay measured by Cell Counting Kit-8 (CCK-8) in U87 MG cells with different concentrations (5, 25, 50 and 100 μg mL^{-1}) of chiral Cys MSN at 24 and 48 h of cell culture. Data are mean ± SEM, experiments were performed in triplicate.

Cys–MSN presented differences in cell uptake and toxicity depending on the functionalized L or D enantiomer, while non-chiral Phe–MSN did not show significant differences.

Effect of chirality in healthy human fibroblast (GM08680)

Additionally, the antiproliferative activity of the nanoparticles were also evaluated in normal human fibroblast (GM08680) cells. Fig. S16 and S17 (ESI†) show that the internalization of Cys-functionalized nanoparticles in healthy cells was much lower than that observed in tumor cells, not exceeding a 16% in any case. What is more, the internalization achieved by D-Cys MSN, which presented greater toxicity in U87, was much lower than L-Cys, suggesting an improvement in the tumor selectivity of the treatment. The low internalization of D-Cys MSN was consistent with the toxicity produced in GM08680, in which cell viability exceeded 90% even 48 h after the addition of the maximum concentration studied (Fig. S18 and S19, ESI†). These data suggest a high antitumor selectivity of D-Cys MSN against healthy cells. As was the case in U87 cells, the addition of achiral nanoparticles functionalized with L/D Phen did not show significant differences in internalization or toxicity (Fig. S20–S23, ESI†).

This journal is © The Royal Society of Chemistry 2021

J. Mater. Chem. B, 2021, **9**, 3544–3553 | **3549**

Effect of chirality on *S. aureus* bacteria

After verifying that the chirality of the Cys particles affected both the viability and internalization into tumor cells, we decided to study whether similar effects can be observed in experiments with bacteria. Regarding targeting to planktonic bacteria, flow cytometry data showed, what seemed a slight increase in internalization for D-Cys MSN (Fig. S24, ESI†). However, when repeating the experiment after the trypan blue addition (Fig. 5), the signal was broadly quenched in all cases (the maximum value obtained being 3.28%), indicating that nanoparticles were on the surface and not inside the bacteria. Possibly because of the large size of the particles, making it difficult to penetrate the bacteria. Equivalent results were obtained when bacteria were incubated in the presence of the L/D Phen functionalized nanoparticles (Fig. S25 and S26, ESI†).
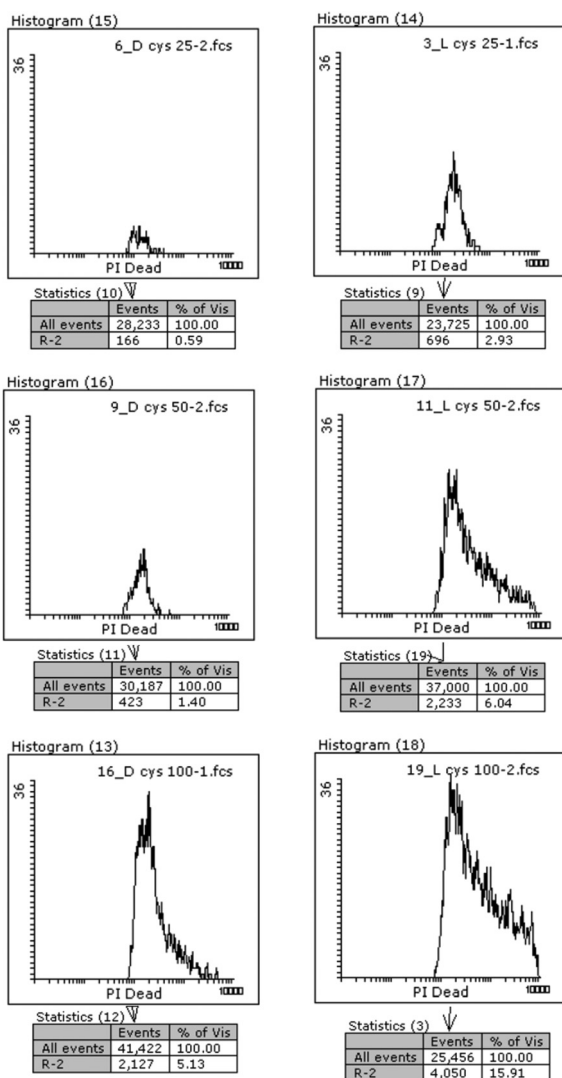
The toxicity of nanoparticles against bacteria was also studied (Fig. S27, ESI†). In this case, and contrary to what happens with the U87 MG cells, L-Cys MSN proved to be more toxic than D-Cys MSN. L-Cys MSN showed a concentration-dependent toxicity, achieving up to 15.9% death at maximum concentration (100 μg mL^{-1}). D-Cys MSN caused a negligible death at concentrations of 25 and 50 μg mL^{-1}, achieving 5.1% when the concentration rises to 100 μg mL^{-1} (Fig. 6).

Fig. 5 Flow cytometry of trypan blue treated *S. aureus* bacteria incubated in the presence to a certain amount (25, 50 and 100 μg mL^{-1}) of fluorescent L-/D-Cys MSN. The yellow fraction is considered F-MSN+ in absence of trypan blue, R1 is the F-MNS+ fraction in the presence of trypan blue.
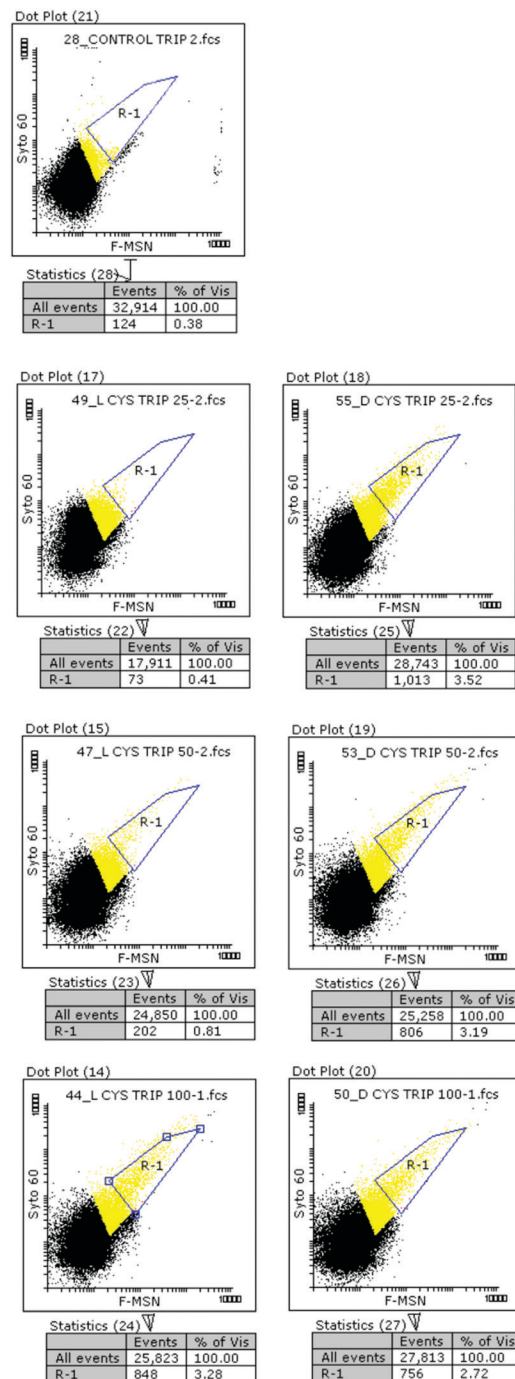

Fig. 6 flow cytometry data of the selected region for dead stained *S. aureus* bacteria. Cell viability was measured using (LIVE/DEAD™ BacLight™ Bacterial Viability Kit).

This data agrees with the study reported by Caldeira *et al.*, in which the biofunctionalization of cellulosic fibres with L-cysteine conferred the material antibacterial properties against *S. aureus*. The mechanism of action that they report is related to cellular metabolism, since incubation with L-Cys causes a decrease from 90% metabolic active cells to 2%.[62] Although, in this study the authors did not explore the chiral properties of cysteine functionalisation but focus only in the L-form. However, Wang *et al.* reported how L-Cys showed preferred antibacterial activity against *S. aureus*, while D-Cys presented stronger antibacterial activity against *E. coli*, *S. enteritis* and *L. monocytogenes*.[63] According to the authors, these differences could be related to structural differences of *S. aureus* cells.[64]

The fact that the same enantiomeric nanoparticle has opposite responses when faced with different biological systems, is not exclusive to the present nanosystem. In previous studies, our research group showed that while D-Cys ZnS:Mn QDs is more toxic to A549 cells,[57] L-form CdSe/ZnS QDs present the highest internalization and toxicity against Ehrlich ascites carcinoma cells.[65] On the other hand, the toxicity study carried out with the NPs containing Phen, resulted again in the absence of differences between samples functionalized with both enantiomeric forms (Fig. S28, ESI†).
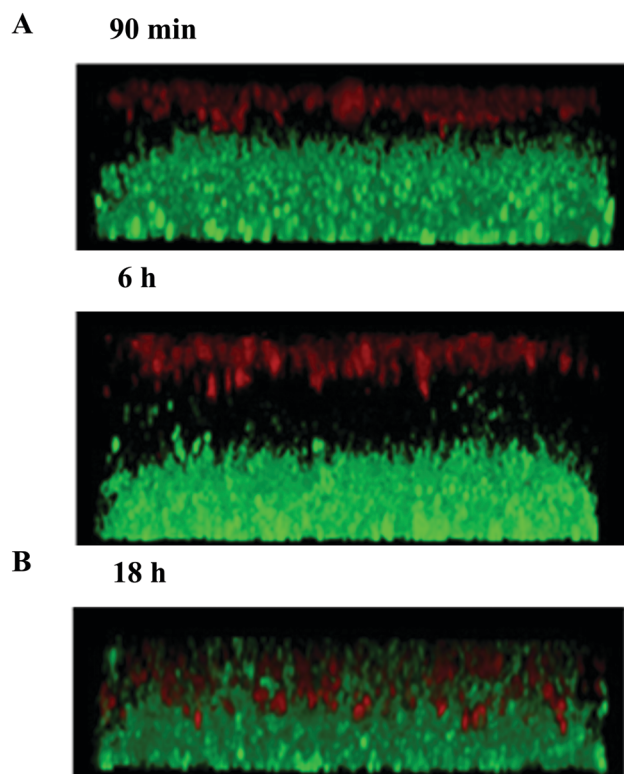
The final step involved evaluating the bacterial biofilm targeting efficacy of the chiral nanoparticles. Plain nanoparticles (R-MSN), with a ζ-potential similar to that of the functionalized particles, were used as a control. To visualize the nanoparticles, they were labelled in red by loading rhodamine B (R) into the pores. For this purpose, a preformed mature biofilm of *S. aureus* expressing GFP was incubated with 100 μg mL^{-1} of each type of nanoparticles suspension for 90 min or 6 h (Fig. 7A).

According to 3D confocal reconstruction there were no significant penetration differences between D/L-Cys MSN and D/L-Phen MSN nor with the control particles. All type of nanoparticles presented the same pattern of penetration. After 90 min of incubation the nanoparticles were deposited on the top of the biofilm, but no penetration inside the biofilm was observed. Again, after 6 h, the particles remained deposited on the surface of the biofilm although in this case a greater separation between the nanoparticles and the bacteria was observed. This is most likely due to a layer of extracellular DNA, protein and other extracellular matter that the bacteria expulse in stress conditions.

In contrast, when the particles were added to an early-stage biofilm (6 h biofilm) and incubated for a further 18 h, the penetration inside the biofilm was observed for all nanoparticle types (Fig. 7B). These results show that the chirality of our silica nanoparticles does not affect penetration into the *S. aureus* biofilm.

Conclusions

In this work we have studied the effect that Cys functionalized MSN chirality has on different biological systems. Besides, the results have been compared with those obtained for non-chiral Phen functionalized NPs.

It has been observed that chirality plays a pronounced role in behavior of U87 tumor cells, showing greater internalization and toxicity in the case of D-Cys MSN. On the other hand, in GM08680 healthy cells, L-Cys presents greater internalization and toxicity, suggesting that D-Cys MSN could be a selective and effective treatment to combat neuroblastoma. Internalization against *S. aureus* proved to be negligible and independent of chirality, possibly because the size of the nanoparticles is comparable to that of bacteria. However, L-Cys MSN seems to have a greater antibiotic character against *S. aureus* causing a greater decrease in the viability of the bacterial population after 2 h of incubation.

In contrast, when the same experiments were carried out with L/D-Phen NPs, no significant differences were observed in either internalization or toxicity in U87 cells, GM08680 MG cells and bacteria, proving the important role that chirality plays in both phenomena.

Finally, the internalization of the nanoparticles in the biofilm was followed up, showing no differences dependent on chirality and, achieving in both cases a certain degree of penetration at 18 h.

The present work highlights the importance of characterise the cell-interaction of chiral nanomaterials in different bio-

Fig. 7 Confocal microscope monitoring of the pattern of penetration into *S. aureus* biofilm expressing GFP, shown for all type of nanoparticles (R-MSN, R-L/D-Cys MSN and R-L/D-Phen). The example presented here is of R-MSN. (A) Mature biofilms were grown for 18 h and then incubated with nanoparticles for 90 min or 6 h as indicated. (B) Early stage biofilms (6 h) were incubated with nanoparticles for 18 h.

This journal is © The Royal Society of Chemistry 2021

J. Mater. Chem. B, 2021, **9**, 3544–3553 | **3551**

logical systems and takes a step forward to further the advancement of nanobiotechnology, nanotoxicology, nanomedicine and other relevant areas.

Conflicts of interest

There are no conflicts to declare.

Acknowledgements

References

1 H. S. Choi and J. V. Frangioni, *Mol. Imaging*, 2010, **9**, 291–310.

2 M. Elsabahy and K. L. Wooley, *Chem. Soc. Rev.*, 2012, **41**, 2545–2561.

3 A. K. Gupta and M. Gupta, *Biomaterials*, 2005, **26**, 3995–4021.

4 E. Roduner, *Chem. Soc. Rev.*, 2006, **35**, 583–592.

5 L. Peng, Y. Liang, X. Zhong, Z. Liang, Y. Tian, S. Li, J. Liang, R. Wang, Y. Zhong, Y. Shi and X. Zhang, *Int. J. Nanomed.*, 2020, **15**, 1363–1372.

6 W. Zhang, R. Taheri-Ledari, Z. Hajizadeh, E. Zolfaghari, M. R. Ahghari, A. Maleki, M. R. Hamblin and Y. Tian, *Nanoscale*, 2020, **12**, 3855–3870.

7 J. R. Francica, R. Laga, G. M. Lynn, G. Mužíková, L. Androvič, B. Aussedat, W. E. Walkowicz, K. Padhan, R. A. Ramirez-Valdez, R. Parks, S. D. Schmidt, B. J. Flynn, Y. Tsybovsky, G. B. E. Stewart-Jones, K. O. Saunders, F. Baharom, C. Petrovas, B. F. Haynes and R. A. Seder, *PLoS Biol.*, 2019, **17**, e3000328.

8 M. Martínez-Carmona, D. Lozano, A. Baeza, M. Colilla and M. Vallet-Regí, *Nanoscale*, 2017, **9**(41), 15967–15973.

9 Y. Pei, M. Li, Y. Hou, Y. Hu, G. Chu, L. Dai, K. Li, Y. Xing, B. Tao, Y. Yu, C. Xue, Y. He, Z. Luo and K. Cai, *Nanoscale*, 2018, **10**, 11418–11429.

10 C. Chen, W. Yao, W. Sun, T. Guo, H. Lv, X. Wang, H. Ying, Y. Wang and P. Wang, *Int. J. Biol. Macromol.*, 2019, **122**, 1090–1099.

11 C. Wang, M. Han, X. Liu, S. Chen, F. Hu, J. Sun and H. Yuan, *Int. J. Nanomed.*, 2019, **14**, 1503–1517.

12 R. Bentley, *Reviews in Cell Biology and Molecular Medicine*, American Cancer Society, 2006.

13 W. Utembe, *Toxicol. Lett.*, 2019, **311**, 58–65.

14 G. Blaschke, H. P. Kraft, K. Fickentscher and F. Köhler, *High Tech–Neue Gesicht Arzneimittelforsch.*, 1979, **29**, 1640–1642.

15 V. Kuznetsova, Y. Gromova, M. Martinez-Carmona, F. Purcell-Milton, E. Ushakova, S. Cherevkov, V. Maslov and Y. K. Gun'ko, *Nanophotonics*, 2021, **10**, 797–824.

16 K. Lv, L. Zhang, W. Lu and M. Liu, *ACS Appl. Mater. Interfaces*, 2014, **6**, 18878–18884.

17 A. Motealleh, P. Dorri, A. H. Schäfer and N. S. Kehr, *Biofabrication*, 2019, **11**, 35022.

18 A. Motealleh, H. Hermes, J. Jose and N. S. Kehr, *Nanomedicine*, 2018, **14**, 247–256.

19 N. S. Kehr and J. Jose, *Appl. Surf. Sci.*, 2017, **425**, 432–439.

20 A. Nandi, C. Ghosh, A. Bajpai and S. Basu, *J. Mater. Chem. B*, 2019, **7**, 4191–4197.

21 N. S. Kehr, *Colloids Surf., B*, 2017, **159**, 125–130.

22 A. Motealleh and N. Seda Kehr, *ACS Appl. Mater. Interfaces*, 2017, **9**, 33674–33682.

23 Y. Li, Y. Zhou, H. Y. Wang, S. Perrett, Y. Zhao, Z. Tang and G. Nie, *Angew. Chem., Int. Ed.*, 2011, **50**, 5860–5864.

24 J. Deng, S. Wu, M. Yao and C. Gao, *Sci. Rep.*, 2016, **6**, 31595.

25 W. Wang, C. Hao, M. Sun, L. Xu, X. Wu, C. Xu and H. Kuang, *Adv. Funct. Mater.*, 2018, **28**, 1805112.

26 Y. Huang, Y. Fu, M. Li, D. Jiang, C. J. Kutyreff, J. W. Engle, X. Lan, W. Cai and T. Chen, *Angew. Chem., Int. Ed.*, 2020, **59**, 4406–4414.

27 X. Zhao, S.-Q. Zang and X. Chen, *Chem. Soc. Rev.*, 2020, **49**, 2481–2503.

28 W. Ma, L. Xu, L. Wang, C. Xu and H. Kuang, *Adv. Funct. Mater.*, 2019, **29**, 1805512.

29 I. E. Palamà, F. Di Maria, M. Zangoli, S. D'Amone, G. Manfredi, J. Barsotti, G. Lanzani, L. Ortolani, E. Salatelli, G. Gigli and G. Barbarella, *RSC Adv.*, 2019, **9**, 23036–23044.

30 F. Liu, H. Zhang, J. Cheng, J. Hu, C. He, Q. Zhang and G. Zou, *Soft Matter*, 2019, **15**, 2051–2056.

31 Q. Xin, Q. Liu, L. Geng, Q. Fang and J. R. Gong, *Adv. Healthcare Mater.*, 2017, **6**, 1601011.

32 F. Li, Y. Li, X. Yang, X. Han, Y. Jiao, T. Wei, D. Yang, H. Xu and G. Nie, *Angew. Chem., Int. Ed.*, 2018, **57**, 2377–2382.

33 M. Martínez-Carmona, Y. Gun'ko and M. Vallet-Regí, *Pharmaceutics*, 2018, **10**, 279.

34 M. Martínez-Carmona, I. Izquierdo-Barba, M. Colilla and M. Vallet-Regí, *Acta Biomater.*, 2019, **96**, 547–556.

35 M. Martínez-Carmona, M. Colilla and M. Vallet-Regí, *Nanomaterials*, 2015, **5**, 1906–1937.

36 M. Hülsemann, C. Zafiu, K. Kühbach, N. Lühmann, Y. Herrmann, L. Peters, C. Linnartz, J. Willbold, K. Kravchenko, A. Kulawik, S. Willbold, O. Bannach and D. Willbold, *J. Alzheimer's Dis.*, 2016, **54**, 79–88.

37 J. E. Rosen and F. X. Gu, *Langmuir*, 2011, **27**, 10507–10513.

38 Y. Guo, L. Wu, K. Gou, Y. Wang, B. Hu, Y. Pang, S. Li and H. Li, *Microporous Mesoporous Mater.*, 2020, **294**, 109862.

39 N. Fan, R. Liu, P. Ma, X. Wang, C. Li and J. Li, *Colloids Surf., B*, 2019, **176**, 122–129.

40 R. S. Li, P. F. Gao, H. Z. Zhang, L. L. Zheng, C. M. Li, J. Wang, Y. F. Li, F. Liu, N. Li and C. Z. Huang, *Chem. Sci.*, 2017, **8**, 6829–6835.

41 N. S. Kehr, *Biomacromolecules*, 2016, **17**, 1117–1122.

42 N. S. Kehr, H.-J. Galla, K. Riehemann and H. Fuchs, *RSC Adv.*, 2015, **5**, 5704–5710.

43 J. El-Gindi, K. Benson, L. De Cola, H.-J. Galla and N. Seda Kehr, *Angew. Chem., Int. Ed.*, 2012, **51**, 3716–3720.

44 P. Voort, I. Gillis-D'Hamers, K. C. Vrancken and E. Vansant, *J. Chem. Soc., Faraday Trans.*, 1991, **87**, 3899–3905.

45 J. L. Paris, M. Colilla, I. Izquierdo-Barba, M. Manzano and M. Vallet-Regí, *J. Mater. Sci.*, 2017, **52**, 8761–8771.

46 F. K. Shieh, C. T. Hsiao, J. W. Wu, Y. C. Sue, Y. L. Bao, Y. H. Liu, L. Wan, M. H. Hsu, J. R. Deka and H. M. Kao, *J. Hazard. Mater.*, 2013, **260**, 1083–1091.

47 E. O'Neill, C. Pozzi, P. Houston, D. Smyth, H. Humphreys, D. A. Robinson and J. P. O'Gara, *J. Clin. Microbiol.*, 2007, **45**, 1379–1388.

48 M. Grün, I. Lauer and K. K. Unger, *Adv. Mater.*, 1997, **9**, 254–257.

49 Y. Lv, J. Li, H. Chen, Y. Bai and L. Zhang, *Int. J. Nanomed.*, 2017, **12**, 4361–4370.

50 J. Ge and Y. Yin, *Adv. Mater.*, 2008, **20**, 3485–3491.

51 T. Ito, L. Sun, M. A. Bevan and R. M. Crooks, *Langmuir*, 2004, **20**, 6940–6945.

52 J. K. Choi, B. E. Haynie, U. Tohgha, L. Pap, K. W. Elliott, B. M. Leonard, S. V. Dzyuba, K. Varga, J. Kubelka and M. Balaz, *ACS Nano*, 2016, **10**, 3809–3815.

53 J. Kuno, Y. Imamura, M. Katouda, M. Tashiro, T. Kawai and T. Nakashima, *Angew. Chem., Int. Ed.*, 2018, **57**, 12022–12026.

54 V. A. Kuznetsova, E. Mates-Torres, N. Prochukhan, M. Marcastel, F. Purcell-Milton, J. O'Brien, A. K. Visheratina, M. Martinez-Carmona, Y. Gromova, M. Garcia-Melchor and Y. K. Gun'ko, *ACS Nano*, 2019, **13**, 13560–13572.

55 M. Martínez-Carmona, Q. P. Ho, J. Morand, A. García, E. Ortega, L. C. S. Erthal, E. Ruiz-Hernandez, M. D. Santana, J. Ruiz, M. Vallet-Regí and Y. K. Gun'ko, *Inorg. Chem.*, 2020, **59**, 10275–10284.

56 S. Busetto, E. Trevisan, P. Patriarca and R. Menegazzi, *Cytometry, Part A*, 2004, **58A**, 201–206.

57 V. A. Kuznetsova, A. K. Visheratina, A. Ryan, I. V. Martynenko, A. Loudon, C. M. Maguire, F. Purcell-Milton, A. O. Orlova, A. V. Baranov, A. V. Fedorov, A. Prina-Mello, Y. Volkov and Y. K. Gun'Ko, *Chirality*, 2017, **29**, 403–408.

58 Y. Ye, J. Liu, M. Chen, L. Sun and M. Lan, *Environ. Toxicol. Pharmacol.*, 2010, **29**, 131–137.

59 W. Lin, Y.-W. Huang, X.-D. Zhou and Y. Ma, *Toxicol. Appl. Pharmacol.*, 2006, **217**, 252–259.

60 J.-S. Chang, K. L. B. Chang, D.-F. Hwang and Z.-L. Kong, *Environ. Sci. Technol.*, 2007, **41**, 2064–2068.

61 R. Krętowski, M. Kusaczuk, M. Naumowicz, J. Kotyńska, B. Szynaka and M. Cechowska-Pasko, *Nanomaterials*, 2017, **7**, 230.

62 E. Caldeira, E. Piskin, L. Granadeiro, F. Silva and I. C. Gouveia, *J. Biotechnol.*, 2013, **168**, 426–435.

63 H. Wang, J. Qian, J. Gu, W. Yan and J. Zhang, *Biochem. Biophys. Res. Commun.*, 2019, **512**, 505–510.

64 C. Morlot, D. Straume, K. Peters, O. A. Hegnar, N. Simon, A.-M. Villard, C. Contreras-Martel, F. Leisico, E. Breukink, C. Gravier-Pelletier, L. Le Corre, W. Vollmer, N. Pietrancosta, L. S. Håvarstein and A. Zapun, *Nat. Commun.*, 2018, **9**, 3180.

65 I. V. Martynenko, V. A. Kuznetsova, I. K. Litvinov, A. O. Orlova, V. G. Maslov, A. V. Fedorov, A. Dubavik, F. Purcell-Milton, Y. K. Gun'ko and A. V. Baranov, *Nanotechnology*, 2016, **27**, 075102.

This journal is © The Royal Society of Chemistry 2021

J. Mater. Chem. B, 2021, **9**, 3544–3553 | **3553**